INTERNATIONAL JOURNAL OF MARITIME TECHNOLOGY
IJMT Vol.19 / Winter & Spring 2024 (32-42)
Available online at: www. ijmt.ir

Frequency Domain Optimization of Homogeneous Anechoic Multi-Layers Using Genetic Programming

Sayed Hamid Sohrabi[1*], Saeed Parsamehr[2], Amir Karimi[2]

[1] *PhD, Mechanical Engineering Department, Malek-Ashtar University of Technology, Isfahan, Iran, Email: s.h.sohrabi@mut-es.ac.ir.*
[2] *MSc, Mechanical Engineering Department, Isfahan University of Technology, Isfahan, Iran, Email: s.parsamehr@alumni.iut.ac.ir*
[3] *PhD student, Mechanical Engineering Department, Isfahan University of Technology, Isfahan, Iran.*

ARTICLE INFO

Article History:
Received: 10 Jun 2023
Accepted: 07 Feb 2024
Available online: 11 Feb 2024

Keywords:
Sound Absorption
Imperialistic Competitive Algorithm (ICA)
Genetic Programming (GP)
Transfer Matrix Method (TMM)
Frequency Domain
Anechoic
Multi-Layer

ABSTRACT

Sound-absorbing coatings are of great importance in noise control, thus to make them technically and economically effective, their design optimization is a necessity. Multi-layered homogeneous linings, intended to provide a certain level of absorption, have recently been of much interest among the anechoic coatings. In the present work, first a mathematical model, called Transfer Matrix Method (TMM) is introduced and validated to properly predict the acoustic response of cavity-less multi-layers. Next, a two-loop optimization technique aimed at maximizing the mean value of echo reduction and minimizing the layers' total thickness is developed. The outer loop (GP) focuses on the number and order of the layers, while the inner (ICA) is dedicated to thickness modification of each layer. Finally, results are demonstrated for some specific cases, where promising solutions are found for different constraints and conditions. As an example, comparing a homogeneous coating invented by the GP-ICA (#Generation 50 of Section 5.3) with a typical cavity-included coating used for sound absorption shows that the thickness of this new coating is reduced by nearly two-thirds (from 50 mm to 18 mm), while the first hit of the 20 dB band of Echo Reduction (ER) has reduced by 65 % (from 20 kHz to 7 kHz), and almost did not fall from this level until the end of the frequency domain of interest (40 kHz). That's while the conventional coating frequency response dropped soon after hitting the 20 dB threshold.

1. Introduction

Automatic optimal design, based on a specific definition of the goals, has been an intriguing field of recent engineering studies [1]. The present paper takes advantage of evolutionary algorithms as an important branch of artificial intelligence to develop a software platform for suggesting sub-optimal premium homogeneous multi-layers for sound absorption. These anechoic coatings are of extensive use in civil and military applications [2]. Although it comes with considerable capabilities, the optimization method called Genetic Programming (GP) is not still widely used in engineering fields. Unlike the conventional use of the GP, which puts various elements (e.g. mathematical operators) in a tree-like structure to form an explicit regression equation [3], in this paper, various rubber materials are put in the single-branched tree structures, thus optimizing the number and order of anechoic layers. Each member of the GP (a multi-layer), separately undergoes a thicknesses optimization as the inner optimization loop, called the Imperialistic Competitive Algorithm (ICA) [4] which is a variant of Genetic algorithms. A simplistic illustration of workflow is provided in Fig 2. The general goal of this two-level algorithm (GP-ICA) is obtaining an anti-detection multi-layer coating, with the highest average level of echo-reduction in a particular frequency range, while keeping the total thickness as low as possible. This two-loop strategy is inspired by [5] where it is argued that the topology construction and parameter value dedication should not be handled in the same strata and how a concurrent optimization of both

topology and parameters is worth complicating the optimization procedure.

It is also noteworthy that the already-existing GPLab toolbox [6] was modified to be harnessed for the special purpose of this paper.
All the layers are essentially made of homogeneous (without holes, also called solid) viscoelastic material, and the powerful analytical method of Transfer Matrices (TMM) [6] is used to simulate their acoustic behavior. The TMM is also used in the literature in conjunction with the GP to achieve an optimal hole-shape design for nonhomogeneous coatings too [7].

In the following, the TMM is first briefly described and verified and finally some typical problems are solved to demonstrate the capabilities of GP-ICA.

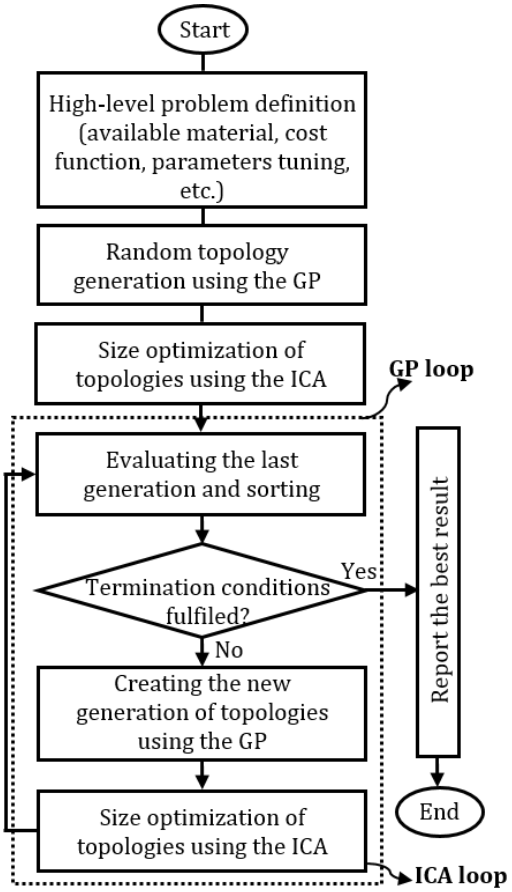

Figure 2. A simplified version of the GP-ICA optimization

2. Mathematical Modeling of Anechoic Layer

Exact and time-efficient modeling of sound-absorbing multi-layers is the key to enabling GP-ICA to propose economic and high-performance coatings. The layers come with different thicknesses and materials. Figure 1 shows a typical multi-layered coating. Reducing the reflection level of the emitted mechanical wave means increasing the Echo Reduction (ER) quantity. The TMM is used to calculate the ER.

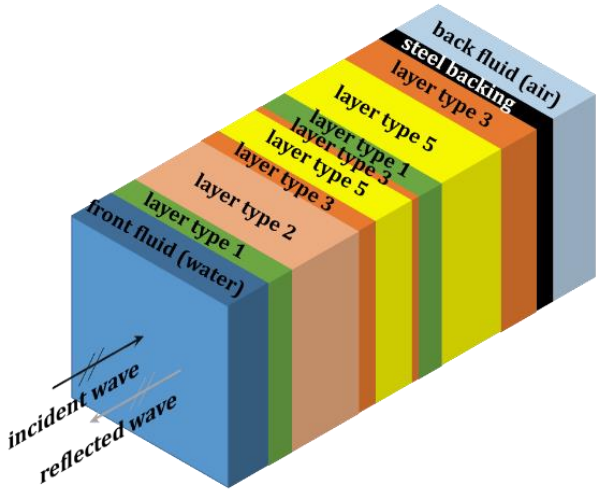

Figure 1. Schematic illustration of a typical multi-layer sound-absorbing coating

3. Governing Equations

The direct analytical approach in evaluating the response of a pressure wave excitation and the resulting wave propagation involves the expression of pressures and stresses in the form of wave potential functions. Then the characteristic equations are formulated by satisfying the boundary conditions in each layer. In [8], this approach is used to formulate the transfer function. The direct method may be useful for the simple single-layered case investigated in [8]; but as the number of layers is increased, the associated algebraic calculations become cumbersome, and inverting the coefficients matrix would be more time-demanding, while some numerical inconveniences may emerge. The Transfer Matrix Method (TMM) was first proposed by Thomson [9] and was surveyed further by others [10-14]. This method is well compatible with computer programming, and therefore, is the best tool to simulate multi-layered coatings and passive acoustic filters. Below is a summary of this method.

In the most general case, the incoming wave forms an angle θ with the y axis and forms an angle ϕ with the z axis, which is located in the xz plane (Figure. 3). As a result, the incoming 2D pressure wave leads to the formation of a three-dimensional stress field. According to in Figure 2, the front and rear layers of this multi-layered coating are in contact with the fluid (assumed non-viscous), and the six state variables used in the TMM matrix of each layer include the axial stress σ_{yy}, shear stress τ_{xy}, vertical particles' velocity V_y and transverse particle velocities V_x,V_z in two sides of every layer. These components are shown in Figure 4.

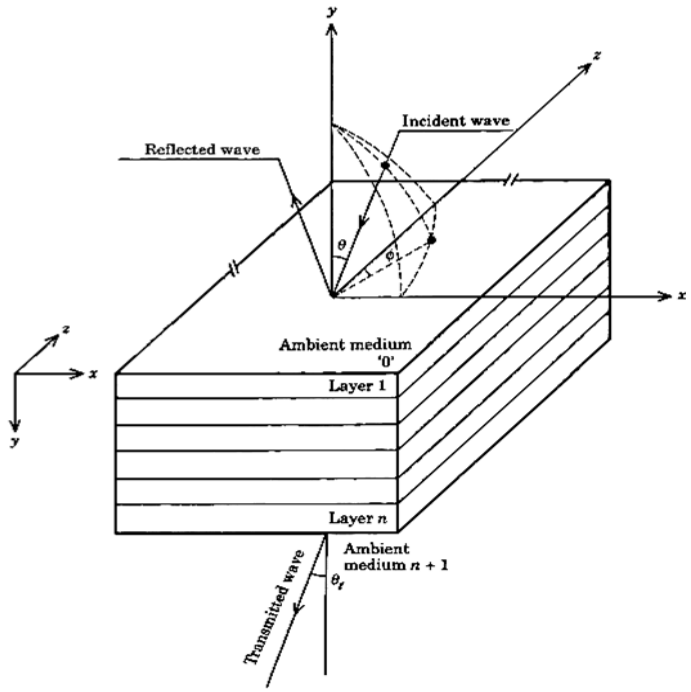

Figure 3. The entrance and exit of the incident wave with a desired angle in a multi-layer coating [15].

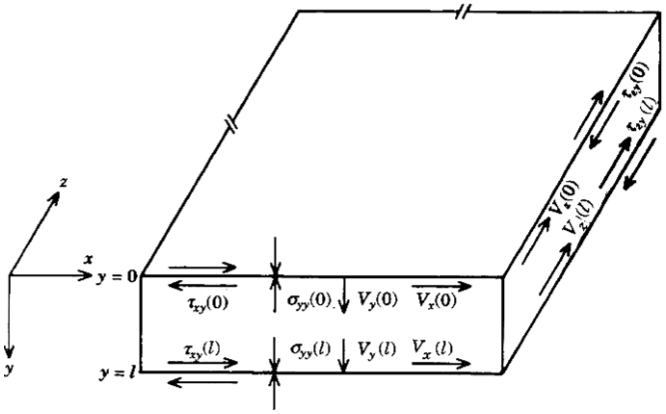

Figure 4. Coordinates and state variables in the upper and lower surface of one of the layers of the multi-layer coating in response to two-dimensional excitation [15].

This general case results in a 6×6 transfer matrix. Multiplying the matrices of every layer leads to an equal transfer matrix, A, representing the total dynamics of the multi-layer coating. As a result, the state variables, S (stresses and velocities) of the first and last layers can be directly linked to each other (Equation (1)).

$$[S]_0 = [A][S]_n$$
$$[A] = [A]_1 \ldots . [A]_{n-1}[A]_n \quad (1)$$

The entries of the A-matrix are described in Appendix B.

The wave enters from the first fluid medium (0^{th} layer) and after passing through n layers (including the viscoelastic blankets and a steel backing) reaches the fluid medium at the end ($n+1^{th}$ layer).

It is assumed that the incident wave establishes a right angle with the anechoic coating. That is because the receiver of the sonar is situated at the same place as the pinger, and if the incident direction is oblique, the reflection wave front will be deviated, making the detection of a submarine even harder (Figure 5). The second reason is that the oblique incidences trigger greater shear waves inside the rubber coating, which is interpreted as more dissipation of the wave energy. Accordingly, the incident wave is considered to be applied at a right angle (critical case), shrinking the transfer matrix dimensions down to 4×4 [16] (See Appendix B).

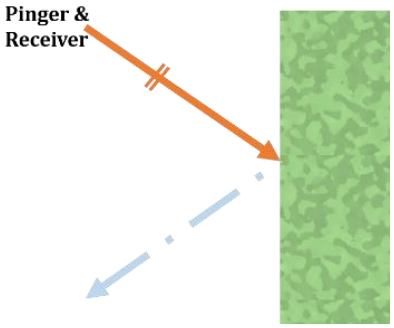

Figure 5. The worst case for a submarine concealing scenario happens when the wave front makes a 90° angle with the coating.

The constituents of the wave propagation moduli, such as transmission, reflection and transmission loss, are nothing but the arrays of the equivalent transmission matrix, which are independent of the "stress and velocity" vector, "S" [15]. This paper utilizes the reflection factor (R) which is calculated as in Equation (2):

$$R = \frac{A_{11}Z_{n+1} + A_{14} - Z_0(A_{41}Z_{n+1} + A_{44})}{A_{11}Z_{n+1} + A_{14} + Z_0(A_{41}Z_{n+1} + A_{44})} \quad (2)$$

where Z_0,Z_{n+1} are the specific impedances of the input and output fluids enclosing the multi-layer coating and the "A_{ij}"s are the arrays of the A-matrix. Finally, the ER is calculated as the following:

$$ER = 20 \log_{10}(1/R) \quad (3)$$

4. Validating the TMM

In order to verify the fidelity of the calculated equations required in the optimization process, namely, the ER (directly calculated from R), some problems with known solutions (benchmarks) have been recalculated by the TMM. The results showed a perfect match, thus validating the correctness of the mathematical basis utilized in the GP-ICA algorithm.

4. 1. Validation Case 1

For the first verification case, a viscoelastic plate with infinite length and width, and a thickness of 20 mm is

considered [17]. This plate is immersed in the enclosing fluid continued to an infinite depth from both sides (Figure 6). The analysis was performed in the frequency range of 2 to 40 kHz and the properties of the viscoelastic layer are as given in Table 1:

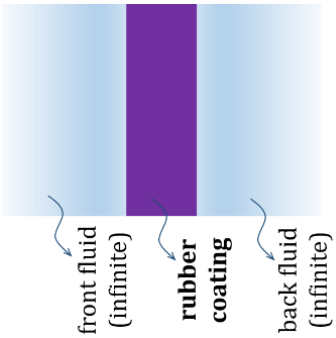

Figure 6. A viscoelastic layer immersed in semi-infinite water medium from both side for the validation case 1

Table 1. properties of the viscoelastic layer in the first verification case [17, 18]

properties	symbol	quantity	unit
Storage modulus	E_r	1.4×10^8	Pa
density	ρ	1100	Kg/m^3
Poisson's ratio	ν	0.49	-
Loss modulus	η	0.23	-

As seen in Figure 7, there is a complete agreement between the results of echo reduction (ER) obtained from the TMM used in this research, and the results in [17].

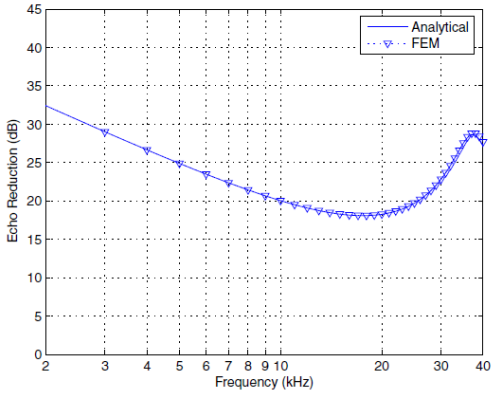

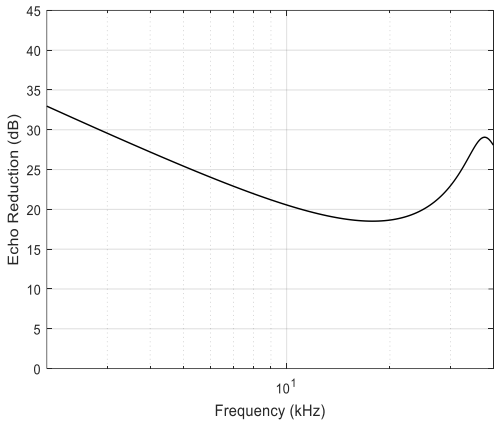

Figure 7. The comparison of ER curves for the Validation Case 1. The reported results [17] (top) are almost identical to those of the TMM (bottom)

4. 2. Validation Case 2

For the second validation case, according to [13], a viscoelastic plate of 40 mm thickness and unlimited length and width is considered. From the front, the plate is in contact with a semi-infinite water environment and a steel backing with a thickness of 5 mm is attached to its back, which is adjacent to a semi-infinite body of air (Figure 8).

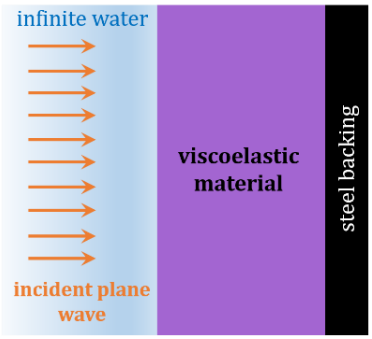

Figure 8. A viscoelastic layer with steel backing for the Validation Case 2 [18].

The analysis is conducted in the frequency range of 1 to 10 kHz. The material properties of the viscoelastic layer are the same as in Table 1. As seen in Figure 9, there is a perfect match between the results of the sound reflection factor obtained from the TMM and the results reported in [18].

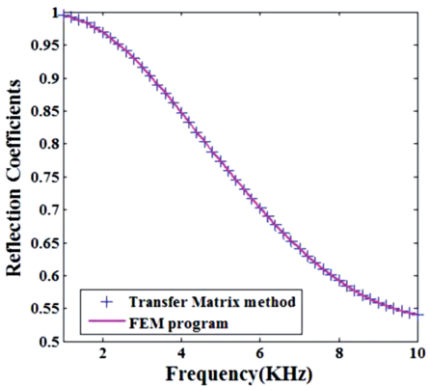

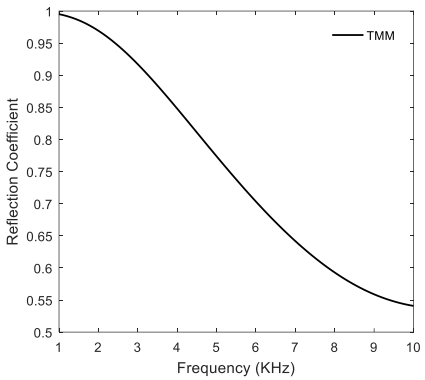

Figure 9. A comparison of the R values between the TMM (bottom) and the reported (top) results [18]

According to the satisfactory results above, the TMM can be considered reliable for simulating the homogeneous sound-absorbing coatings subject to a vertical incident angle. As mentioned before, the worst scenario against stealth occurs at the vertical incidence, where the most reflection towards the receiver (placed at the source of propagation) is expected. This can guarantee the effectiveness of the designs proposed by the GP-ICA for other possible angles of the wave front.

5. Results and discussion

The optimization method used in this paper includes two levels. The higher loop (GP) is intended to conduct a comprehensive search in the unstructured topology space, so as to converge to an optimal topology or arrangement of the layers, while the layers' thicknesses are optimized by a lower-hand algorithm operating in the numerical domain (ICA). Both optimization algorithms are branches of evolutionary processing methods.

In order to demonstrate the capabilities of the GP-ICA software as a powerful tool for designing multi-layer mechanical wave absorbents, some design cases are solved using this computer program. Available constituent materials, the desired frequency range, and the optimization goal are determined for each case. The maximum allowed thickness of coatings (20 mm or 40 mm) are determined per case, also.

There are numerous tuning parameters governing the algorithm, among which:

Number of frequency points calculated for each frequency response = 20

GPLab:
Generations before the algorithm stops = 50
Population size = 70

ICA:
Iterations before the algorithm stops = 4
Population size = 30

Number of empires: 4

More tuning parameters are found in Appendix A.

5. 1. Case 1

In this case, the optimization is to be carried out on a coating with a maximum thickness of 20 mm, and 3 material types are found in the options list (Table 2), while the target frequency ranges from 0 to 20 kHz.

TABLE 2. The library of viscoelastic materials used in optimization case 1

properties	symbol	quantity			unit
		Mat 1	Mat 2	Mat 3	
Storage modulus	E_r	$1.4e8$	$1.8e6$	$3.3e8$	Pa
Density	ρ	1100	1000	1200	Kg/m^3
Poisson's ratio	ν	0.49	0.49975	0.49	-
Loss modulus	η	0.23	0.15	0.8	-

The ER frequency responses associated with the best solutions of the first and last GP generations are compared in Figure 10, which shows significant growth in the latter all over the frequency range. Considering the limited number of material types and the short allowed maximum overall length, the quality of the obtained solution is highly significant.

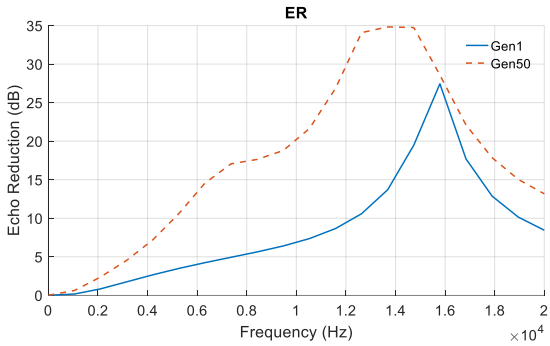

Figure 10. A comparison between the ER frequency responses in the initial and 50th generations (case 1)

The corresponding layers' order and their thicknesses for each coating are depicted in Figure 11. As witnessed, apart from the order and material types, the layers' thicknesses are also modified in the 50th generation, which shows the contribution of both loops of the GP-ICA.

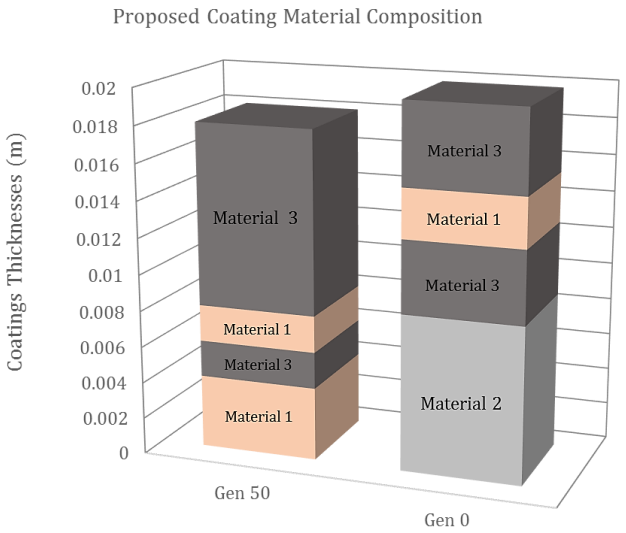

Figure 11. The material type, order, and thicknesses of the coating layers discussed in case 1

Figure 12 illustrates the gradual growth of the solution quality throughout the generations.

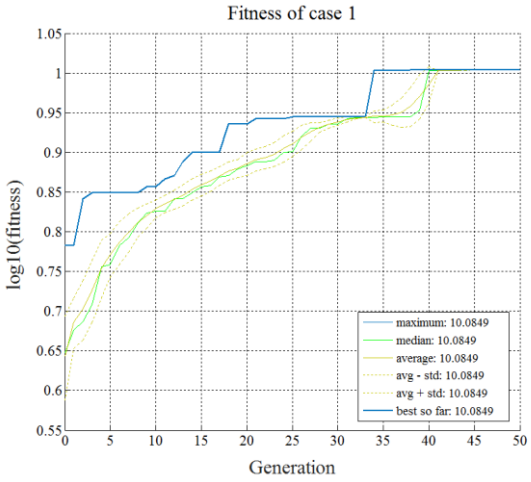

Figure 12. Gradual improvement of the fitness function of case 1

5. 2. Case 2

In this case, the goal is set for the lower frequency range (0.5-5 kHz) and from now on, the material library includes nine viscoelastic (rubber) options (Table 3). Also, if the amount of ER (in decibels) at any frequency is less than a lower non-functionality, or so-called saturation limit, the coating's ability of echo reduction is considered as poor or even worthless in the practical point of view. Accordingly, the points of the graph lying under the lower saturation limit (LSL), are multiplied by 5%, to make the algorithm focus on more useful solutions. Similarly, if somewhere in the frequency range, the ER exceeds the high saturation limit (HSL), the difference between the resulting reduction of echo and the HSL is multiplied by 5% and then added to the HSL. This makes the algorithm reluctant to offer excess quality at some ranges (avoids over-designing). As a rule of thumb, very high levels of ER at some frequency bands, typically impedes the chance of premium results in other parts of the scope. For this case, the LSL and HSL are considered 10 and 20 dBs respectively. This cost function tuning would greatly reduce unnecessary quality improvement.

TABLE 3. The library of viscoelastic materials used in optimization cases 2 to 4

properties	Storage modulus	density	Poisson's ratio	Loss modulus
symbol	E_r	ρ	ν	η
unit	Pa	Kg/m^3	-	-
Mat 1	$1.0e8$	950	0.49	0.2
Mat 2	$4.0e6$	1300	0.49	0.25
Mat 3	$1.4e8$	1000	0.4998	0.15
Mat 4	$1.14e9$	1100	0.49	0.23
Mat 5	$4.14e9$	1400	0.4	0.06
Mat 6	$1.27e8$	1100	0.489	0.2
Mat 7	$7.1e7$	1100	0.494	0.2
Mat 8	$1.5e8$	1350	0.49	0.23
Mat 9	$1.3e8$	1300	0.49	0.23

Figure 13 shows the ER curves for the best members of the 0^{th}, 20^{th}, 40^{th}, and 50^{th} generations. As seen, the 50^{th} generation has tried to obtain the most presence in the desired ER band (10-20 dB). Although the 40^{th} generation has reached the desired band faster, it has faced a relatively unfavorable drop afterwards. In addition, it should be kept in mind that the solution of the 50th generation is 4 mm thinner compared to the 40^{th}. Also, it should be noted that the curves corresponding to the 10^{th} and 30^{th} generations are identical to those of the 20th and 40th generations, respectively, thus they are overlapped and nonvisible

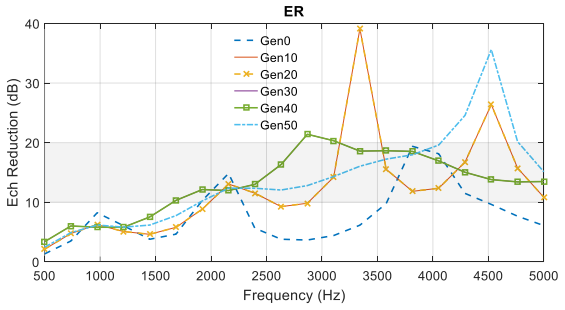

Figure 13. A comparison between the ER frequency responses of various generations (case 2)

The coating layers' order and their thicknesses for case 2 are depicted in Figure 14. The remarkable fact is all of the proposed solutions are relatively thick. This

implies that achieving high-quality solutions at low frequencies requires much greater total thicknesses for the coatings.

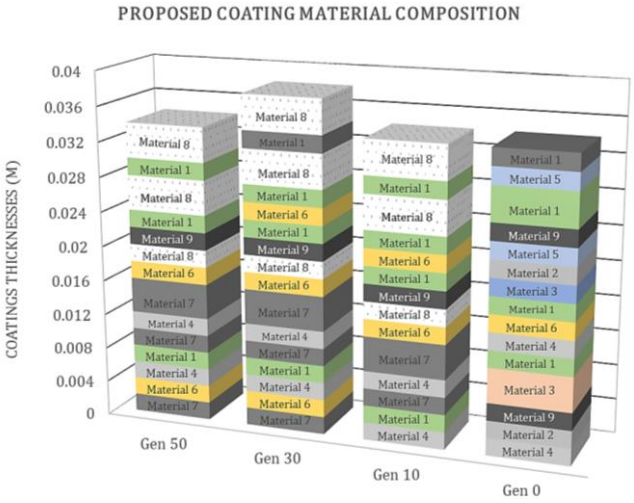

Figure 14. The material type, order, and thicknesses of the coating layers discussed in case 2

5. 3. Case 3

In this case, a wide frequency range (0.5-40 kHz) is targeted, and the LSL and HSL are determined as 10 and 30 dBs respectively. The solutions' graphs are shown for the 0th (initial), 10th, and 50th generations in Figure 15. As witnessed, the algorithm has not obtained any better results from the 20th generation ahead, which means the global optimum is probably reached.

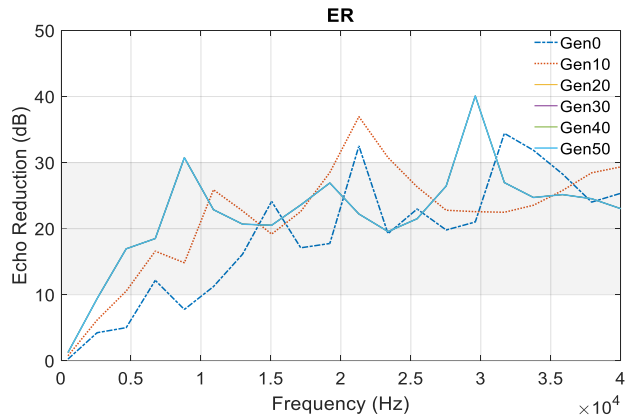

Figure 15. A comparison between the ER curves of various generations (case 3)

As can be seen, the initial solution has no advantage over others, as it has occupied the 10-30 dB band so sparsely, and is even unsuccessful outside this ribbon, while the proposed coating is very thick. On the contrary, the solution in the 50th generation has tried to have the most presence in the desired ER band. Even though the best of the 10th generation has outperformed the 50th in achieving ER levels at some parts of the frequency scope, it cannot be counted as the best, since firstly, the 50th generation has surpassed the 10th in some other areas of the frequency range, and secondly, the 50th has never had an ER level less than 20 dB (twice the minimum necessary), even in the frequencies where it falls behind from the 10th. In addition, the response of the 50th generation at frequencies below 10 kHz has appeared much more successful than other competitors. The thickness of these two solutions are also low and almost equal. According to the above explanations, the 50th solution is counted as the best fit. The coating layers' order and their thicknesses are depicted in Figure 16.

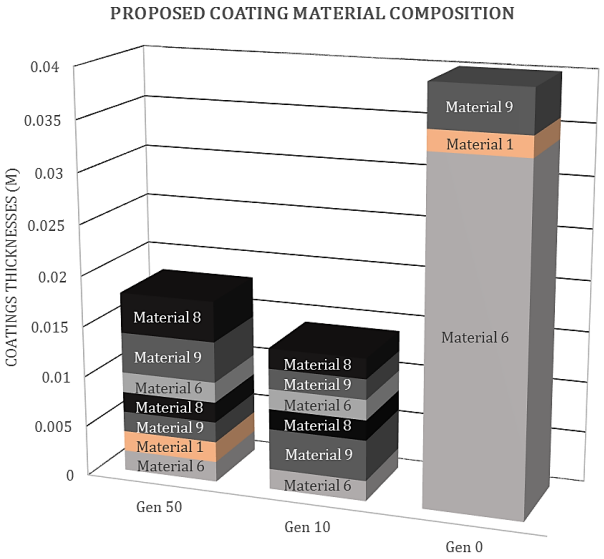

Figure 16. The material type, order, and thicknesses of the coating layers discussed in case 3

5. 4. Case 4

In this case, the lower and upper saturation limits are considered as 10 and 40 dBs, respectively. Figure 17 shows the ER frequency response curves for the best solutions in the 0th, and 50th generations. It is to be noted that after the 10th generation, the results are exactly the same, and their graphs are overlapped.

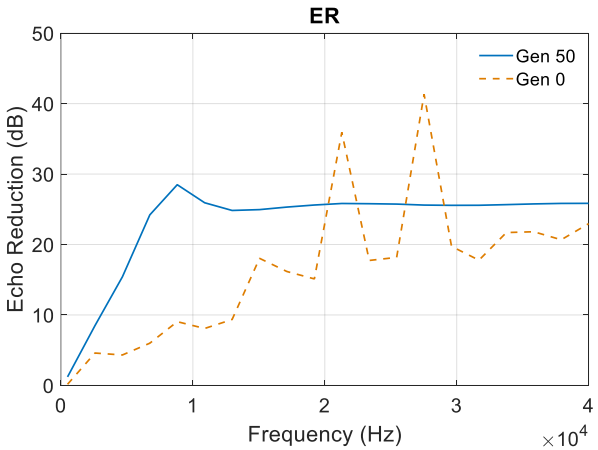

Figure 17. A comparison between the ER curves of various generations (case 4)

Although the initial generation is considered a fair solution as compared to its super-short thickness (Figure 18), especially for the middle frequencies, the 50th generation offers a more suitable suggestion both in terms of the average ER and the quality of the response at low frequencies. Moreover, it has a short thickness compared to the maximum selectable thickness (40 mm). However, overall, the best of this case is not as good as case 3, and it shows choosing the saturation limits, as part of the cost function is of critical importance. For this case, the HSL is set as too high, misleading the optimization core.

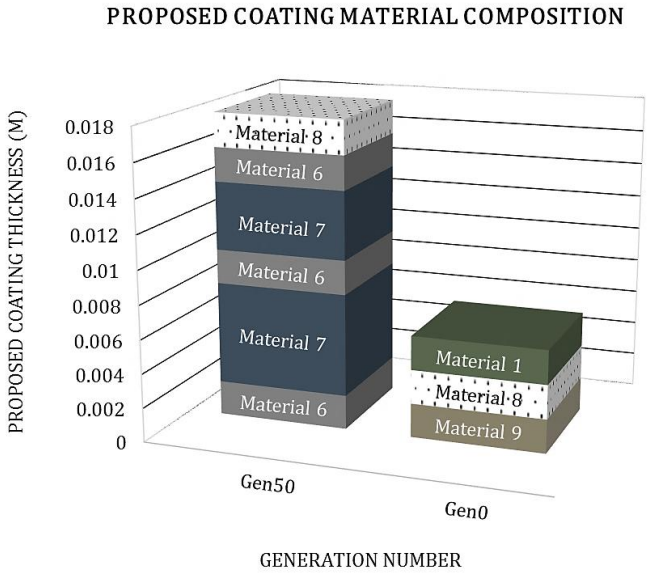

Figure 18. The material type, order, and thicknesses of the coating layers discussed in case 4

5. 5. Discussion

The results generated by the present method are comparable with some prevalent cavity-included coatings such as those presented in the literature [19, 20], in the sense of the ER response levels. Layers incorporating holes, typically show a number of ER peaks at certain frequencies, but perform relatively poor at other frequencies, while homogeneous layers come with less fluctuations during the whole frequency range, and even can demonstrate greater mean values, and thinner total thicknesses, when optimized using algorithms such as the GP-ICA. Figure 16 compares the results of some layers of 50 mm thickness including cylindrical holes and a steel backing of 20 mm ([20]) with the 50th generation of case 3. The curves for different hole sizes are depicted, and as seen, none of the ER responses are as good as the composite coating invented by the GP-ICA, from either the thickness or ER performance criteria. To be precise, the lining thickness is reduced by 64 % (from 50 mm to 18 mm), while the first hit of the 20 dB threshold of ER has reduced by 65 % (from 20 kHz to 7 kHz), and almost did not lose this level until the end of the frequency domain of interest (40 kHz).

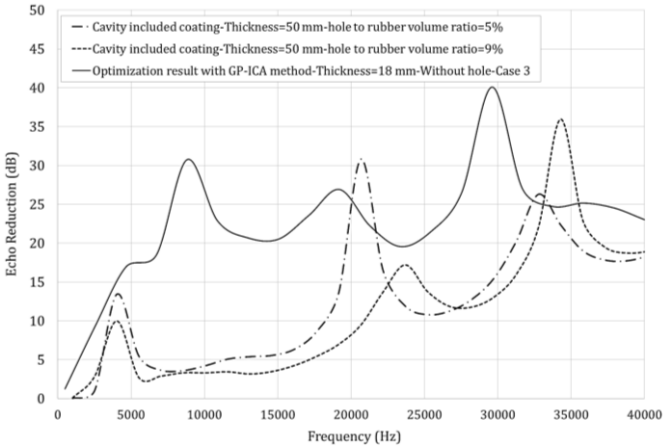

Figure 16. The ER curves of the cavity-included coatings in the 1-40 kHz frequency range for various hole/rubber volume ratios [20] and the optimization result using GP-ICA method (present study, Case 3)

6. Conclusion

The contribution of this research is the development of a flexible and efficient platform for designing immediate, automatic, and optimal multi-layered anti-detection homogeneous coatings in arbitrary frequency ranges. Taking advantage of a combined and two-level optimization method led to interestingly efficient coatings. In this research, a model based on the TMM and a two-loop optimization software (GP-ICA) were provided to analyze, design and optimize all types of multi-layered sound-absorbing coatings. Also, to prove the effectiveness of the proposed model, some verifications were conducted. Therefore, by defining a certain goal (here, the ER) and the desired conditions of the response, the necessary optimizations can be done easily using this computer program. The obtained results show that if the cost function is defined intelligently and based on the real needs of the industry, GP-ICA can effectively search the solution space with fairly low hardware resource requirements. The total thicknesses suggested by the software are thinner than the typical coatings, while the ER levels are even better than the cavity-included sound absorbent coatings, in all frequency bands. Also, the constraints and the design goals may be set for different practical purposes.

7. Appendices

Appendix A

A list of some most important adjustment parameters is provided below. The calibration/selection of these values depends on the computer resource available the conditions of the problem, and determines the way the algorithm evolves throughout the generations. A full understanding of their meaning needs a profound study of the evolutionary mechanics, namely the GP literature.
Each record can take different values from the list, and the item chosen for this article can be distinguished with the **bold** font style:

initpoptype = {'growinit','fullinit','**rampedinit**'};

expected = {'**absolute**','rank85','rank89'};

elitism = {'keepbest','replace','halfelitism','**totalelitism**'};

survival = {'**fixedpopsize**','resources','pivotfixe'};

dynamicresources = {'**0**','1','2'}; % 0=no; 1=normal; 2=heavy

resourcespopsize = {'low','**steady**','free'};

resourcesfitness = {'**normal_accept**','light_accept'};

sampling={'roulette','sus','tournament','**lexictour**','doubletour','sampleall'};

drawperspin = ' **maximum_possible**'; % how many individuals can be drawned per wheel spin

savetofile={'never','firstlast','**every10**','every100','always'};

operatorprobstype = {'fixed','**variable**'};

initialprobstype = {'**fixed**','variable'};

pointmutationtype = {'**1point**','npoint'};

numbackgen = 'posint'; ***This positive integer is determined as '3'**

percentback='special_01float'; *a float between 0 and 1, inclusive; ***This value is determined as '0.25'**

percentchange='01float'; ***This value is determined as '0.25'**

minprob='01float'; *** This value is determined as '0.1'**

depthnodes={'**1**','2'}; *1=limit depth; 2=limit nodes

fixedlevel='**1**'; % use strict limit: 0=no, 1=yes

dynamiclevel={'**0**','1','2'}; *0=no; 1=normal; 2=heavy

inicmaxlevel='posint'; ***This positive integer is determined as '10'**

veryheavy = 'boolean'; ***This 'boolean' is determined as '0'**

defaults.functions = '{''**Type1**'' **1; ''Type2'' 1; ''Type3'' 1; ''Type4'' 1; ''Type5'' 1; ''Type6'' 1; ''Type7'' 1; ''Type8'' 1; ''Type9'' 1;** }'; *This is the material library for the present paper.

Appendix B

The matrix "A" is defined as in Eq. A-1 [10,11]:

$$\begin{matrix} C_L+\frac{2k^2}{k_T^2}(C_T-C_L) & j\left\{\frac{k}{q_L}FS_L-\frac{2kq_T}{k_T^2}S_T\right\} \\ j\left\{\frac{2kq_L}{k_T^2}S_L-\frac{k}{q_T}FS_T\right\} & C_T+\frac{2k^2}{k_T^2}(C_L-C_T) \\ \frac{1}{\rho C_T}\frac{k}{k_T}(C_L-C_T) & \frac{j}{\rho c_T}\left\{\frac{k^2}{k_T q_L}S_L+\frac{q_T}{k_T}S_T\right\} \\ \frac{j}{\rho c_T}\left\{\frac{q_L}{k_T}S_L+\frac{k^2}{k_T q_T}S_T\right\} & \frac{1}{\rho C_T}\frac{k}{k_T}(C_L-C_T) \end{matrix}$$

$$\begin{matrix} \rho C_T\frac{2kF}{k_T}(C_L-C_T) & j\rho c_L\left\{\frac{k_T}{q_L}F^2S_L-\frac{4q_Tk^2}{k_T^3}S_T\right\} \\ j\rho c_T\left\{\frac{4k^2q_L}{k_T^3}S_L+\frac{k_TF^2}{q_T}S_T\right\} & \rho C_T\frac{2kF}{k_T}(C_L-C_T) \\ C_T+\frac{2k^2}{k_T^2}(C_L-C_T) & j\left\{\frac{k}{q_L}FS_L-\frac{2kq_T}{k_T^2}S_T\right\} \\ j\left\{\frac{2kq_L}{k_T^2}S_L-\frac{k}{q_T}FS_T\right\} & C_L+\frac{2k^2}{k_T^2}(C_T-C_L) \end{matrix} \quad \text{(B-1)}$$

where:
τ_{xy} and σ_y are the shear and compressive stresses respectively;
$k.q_L.q_T.k_L.k_T$ are the wavenumbers related by the compatibility equations below (Eq. B-2):

$$q_L=\pm\left(k_L{}^2-k^2\right)^{1/2}\ and\ q_T=\pm\left(k_T{}^2-k^2\right)^{1/2} \quad \text{(B-2)}$$

It is to be noted that the subscript L denotes the longitudinal or dilatational waves, and the subscript T denotes torsional or transverse shear waves.
The capital letters "C"s and "S"s and the "F" are defined as follows (Eq. A-3):

$$\begin{matrix} C_L\equiv\cos(q_Ll)\,.S_L\equiv\sin(q_Ll), \\ C_T\equiv\cos(q_Tl).\ S_T\equiv\sin(q_Tl), \end{matrix} \quad \text{(B-3)}$$

$$F \equiv 1 - 2k^2/{k_T}^2$$

And ρ is the mass density.
Also, c_L and c_T stand for the longitudinal and shear wave speeds, respectively.
And v is the particle speed of the rubber material, j is the imaginary number, and l is the thickness of the rubber coating.
Also, the k_L, k_T are calculated as the following:

$$\begin{aligned} {k_L}^2 &= \left(\frac{\omega}{c_L}\right)^2 = \frac{\omega^2\rho}{G}\frac{1-2\mu}{2-2\mu}, \\ {k_T}^2 &= \left(\frac{\omega}{c_T}\right)^2 = \frac{\omega^2\rho}{G} \end{aligned} \qquad \text{(B-4)}$$

In the case of the right angle radiation, the A-matrix is reduced into:

$$\begin{matrix} C_L & 0 & 0 & j(\rho c_L)S_L \\ 0 & C_T & j(\rho c_T)S_T & 0 \\ 0 & \frac{j}{\rho c_T}S_T & C_T & 0 \\ \frac{j}{\rho c_L}S_L & 0 & 0 & C_L \end{matrix} \qquad \text{(B-5)}$$

8. References.

[1] H. Qiao, P. Huang, D. De Domenico, (2023), Automatic optimal design of passive vibration control devices for buildings using two-level evolutionary algorithm, Journal of Building Engineering, Vol.72, 106684 [https://doi.org/10.1016/j.jobe.2023.106684].

[2] Z. Zhang, Y. Zhao, N. Gao, (2023), Recent study progress of underwater sound absorption coating, Engineering Reports, e12627 [https://doi.org/10.1002/eng2.12627].

[3] M. Sharma, H. Agrawal, B. Choudhary, (2022), Multivariate regression and genetic programming for prediction of backbreak in open-pit blasting, Neural Computing and Applications, 1-12 [https://doi.org/10.1007/s00521-021-06553-y].

[4] E. Atashpaz-Gargari, C. Lucas, (2007), Imperialist competitive algorithm: an algorithm for optimization inspired by imperialistic competition, 2007 IEEE congress on evolutionary computation, Ieee, pp. 4661-4667 [**DOI:**10.1109/CEC.2007.4425083].

[5] S.K. Tabatabaei, S. Behbahani, C.W. de Silva, (2016), Self-adjusting multidisciplinary design of hydraulic engine mount using bond graphs and inductive genetic programming, Engineering Applications of Artificial Intelligence,Vol.48,p.32-39 [DOI:https://doi.org/10.1016/j.engappai.2015.10.010].

[6] S. Silva, J. Almeida, (2003), Gplab-a genetic programming toolbox for matlab, Proceedings of the Nordic MATLAB conference, Citeseer, p. 273-278.

[7] S. Zhou, Z. Fang, (2022), Optimization design of acoustic performance of underwater anechoic coatings, Acoustics Australia, Vol.50, p.297-313 [DOI:https://doi.org/10.1007/s40857-022-00267-4].

[8] S.H. Ko, H.H. Schloemer, (1989), Calculations of turbulent boundary layer pressure fluctuations transmitted into a viscoelastic layer, The Journal of the Acoustical Society of America, Vol.85, p.1469-1477 [DOI:https://doi.org/10.1121/1.397347].

[9] W.T. Thomson, (1950), Transmission of elastic waves through a stratified solid medium, Journal of applied Physics, Vol.21, p. 89-93 [DOI:https://doi.org/10.1063/1.1699629].

[10] N.A. Haskell, (1990), The dispersion of surface waves on multilayered media, Vincit Veritas: A Portrait of the Life and Work of Norman Abraham Haskell, 1905–1970,Vol. 30, p. 86-103 [DOI:https://doi.org/10.1029/SP030p0086].

[11] E.C. Pestel, F.A. Leckie, E. Kurtz, (1964), Matrix methods in elastomechanics, Journal of Applied Mechanics, Vol. 31, 574 [DOI:10.1115/1.3629714].

[12] M. Munjal, (1975), Velocity ratio-cum-transfer matrix method for the evaluation of a muffler with mean flow, Journal of sound and Vibration, Vol. 39, p. 105-119 [DOI:https://doi.org/10.1016/S0022-460X(75)80211-2].

[13] D. Folds, C. Loggins, (1977), Transmission and reflection of ultrasonic waves in layered media, The Journal of the Acoustical Society of America, Vol.62, 1102-1109 [DOI:https://doi.org/10.1121/1.381643].

[14] P.R. Stepanishen, B. Strozeski, (1982), Reflection and transmission of acoustic wideband plane waves by layered viscoelastic media, The Journal of the Acoustical Society of America, Vol.71, p. 9-21 [DOI: https://doi.org/10.1121/1.387249].

[15] J. Sastry, M. Munjal, (1995), A transfer matrix approach for evaluation of the response of a multi-layer infinite plate to a two-dimensional pressure excitation, Journal of sound and vibration, Vol. 182 p. 109-128 [DOI: https://doi.org/10.1006/jsvi.1995.0185].

[16] M. Munjal, (1993), Response of a multi-layered infinite plate to an oblique plane wave by means of transfer matrices, Journal of Sound and Vibration, Vol.162, p. 333-343 [DOI: https://doi.org/10.1006/jsvi.1993.1122].

[17] S. Panigrahi, C. Jog, M. Munjal, (2008), Multi-focus design of underwater noise control linings based on finite element analysis, Applied acoustics, Vol.69, p. 1141-1153 [DOI: https://doi.org/10.1016/j.apacoust.2007.11.012].

[18] J. Li, S. Li, (2018), Topology optimization of anechoic coating for maximizing sound absorption, Journal of Vibration and Control, Vol. 24, p. 2369-2385[DOI:https://doi.org/10.1177/1077546316685678].

[19] S.H. Sohrabi, M.J. Ketabdari, (2018), Numerical simulation of a viscoelastic sound absorbent coating with a doubly periodic array of cavities, Cogent Engineering, Vol. 5, 1529721 [DOI: https://doi.org/10.1080/23311916.2018.1529721].

[20] S.H. Sohrabi, M.J. Ketabdari, (2020), Stochastic modeling and sensitivity analysis of underwater sound absorber rubber coating, Applied Acoustics, Vol. 164, 107282 [DOI: https://doi.org/10.1016/j.apacoust.2020.107282].